Geochemical Perspectives Letters

Onset of new, progressive crustal growth in the central Slave craton at 3.55 Ga

J.R. Reimink[1*], D.G. Pearson[2], S.B. Shirey[1], R.W. Carlson[1], J.W.F. Ketchum[3]

OPEN ACCESS
doi: 10.7185/geochemlet.1907

Abstract

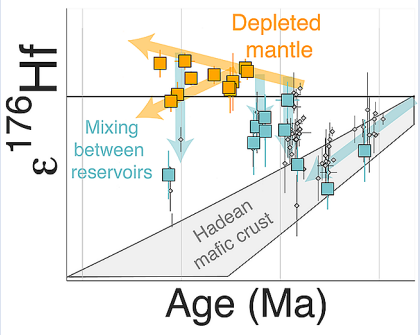

Ancient rock samples are limited, hindering the investigation of the processes operative on the Earth early in its history. Here we present a detailed study of well-exposed crustal remnants in the central Slave craton that formed over a 1 billion year magmatic history. The tonalitic-granodioritic gneisses analysed here are broadly comparable to common suites of rocks found in Archean cratons globally. Zircon Hf isotope data allow us to identify a major change positive εHf starting at ~3.55 Ga. The crust production processes and spatial distribution of isotopic compositions imply variable interaction with older crust, similar to the relationships seen in modern tectonic settings; specifically, long-lived plate margins. A majority of the Slave craton might have been formed by a similar mechanism.

Received 1 November 2018 | Accepted 20 February 2019 | Published 28 March 2019

Introduction

The growth and preservation of Earth's continental crust is an important planetary differentiation process. The Eo- to Mesoarchean is an important era when crustal preservation was just beginning to become successful. Crust from this period is the only vestige that remains to evaluate early geodynamics, the evolution of the atmosphere and ocean chemistry, and ultimately, the origin of life. Though many recent models suggest that a large fraction of the present crust formed in the Archean (*e.g.*, Dhuime *et al.*, 2015), details of the timing of its extraction from the mantle and the mechanism of continental growth remain unclear, in part because of an incomplete rock record in many areas. Here we study an ancient crustal terrane that preserves an exceptionally long record of crustal production, allowing us to track the geodynamic processes of crust formation for over 1.5 Gyr.

Archean cratons are blocks of stable continental crust >2.5 billion years old, forming the cores of Earth's most ancient continents. The Slave craton of the Northwest Territories, Canada is an archetypal example, with extensive exposures of Meso- to Palaeoarchean rocks, making it ideally suited for tracing crust formation and reworking in the Archean.

The core of the Slave craton—the Central Slave Basement Complex (CSBC; Bleeker *et al.*, 1999a,b)—consists of extensive exposures of basement gneiss thought to extend even farther beneath younger granitoids (Davis and Hegner, 1992; Thorpe *et al.*, 1992; Fig. 1). Although other cratons are also endowed with basement gneiss complexes (*e.g.*, Moyen and Martin, 2012), the Slave craton is exceptional for the age range of exposed crust within a coherent geographic area. The detailed petrologic and tectonic framework for the formation of the Acasta Gneiss Complex (AGC) from 4.02 to 3.4 Ga (*e.g.*, Reimink *et al.*, 2018 and references therein) can be used to explore how the younger, more geographically expansive, CSBC is related to the AGC in the subsequent billion years of crustal evolution. The new data presented here from both younger AGC samples (3.4–2.94 Ga) as well as a suite of 3.4–2.9 Ga CSBC samples, allow direct examination of the evolution of the broader Slave craton.

Geology and Geochemistry of the Slave Basement Gneisses

The definition of the CSBC (Bleeker *et al.*, 1999a) encompasses the zone of exposed basement gneisses in the central to south-central portion of the craton, including the Acasta Gneiss Complex. However, we refer to the CSBC and AGC independently to compare their formational mechanisms. The Acasta Gneiss Complex, on the westernmost margin of the Slave craton (Fig. 1), has received by far the most scientific interest due to the presence of the oldest known zircon-bearing

1. Department of Terrestrial Magnetism, Carnegie Institution for Science, Washington DC, 20015, USA
2. Department of Earth and Atmospheric Sciences, University of Alberta, Edmonton, AB, Canada T6G2E3
3. Northwest Territories Geological Survey, Yellowknife, NT, Canada X1A1K3
* Corresponding author (email: jreimink@carnegiescience.edu)

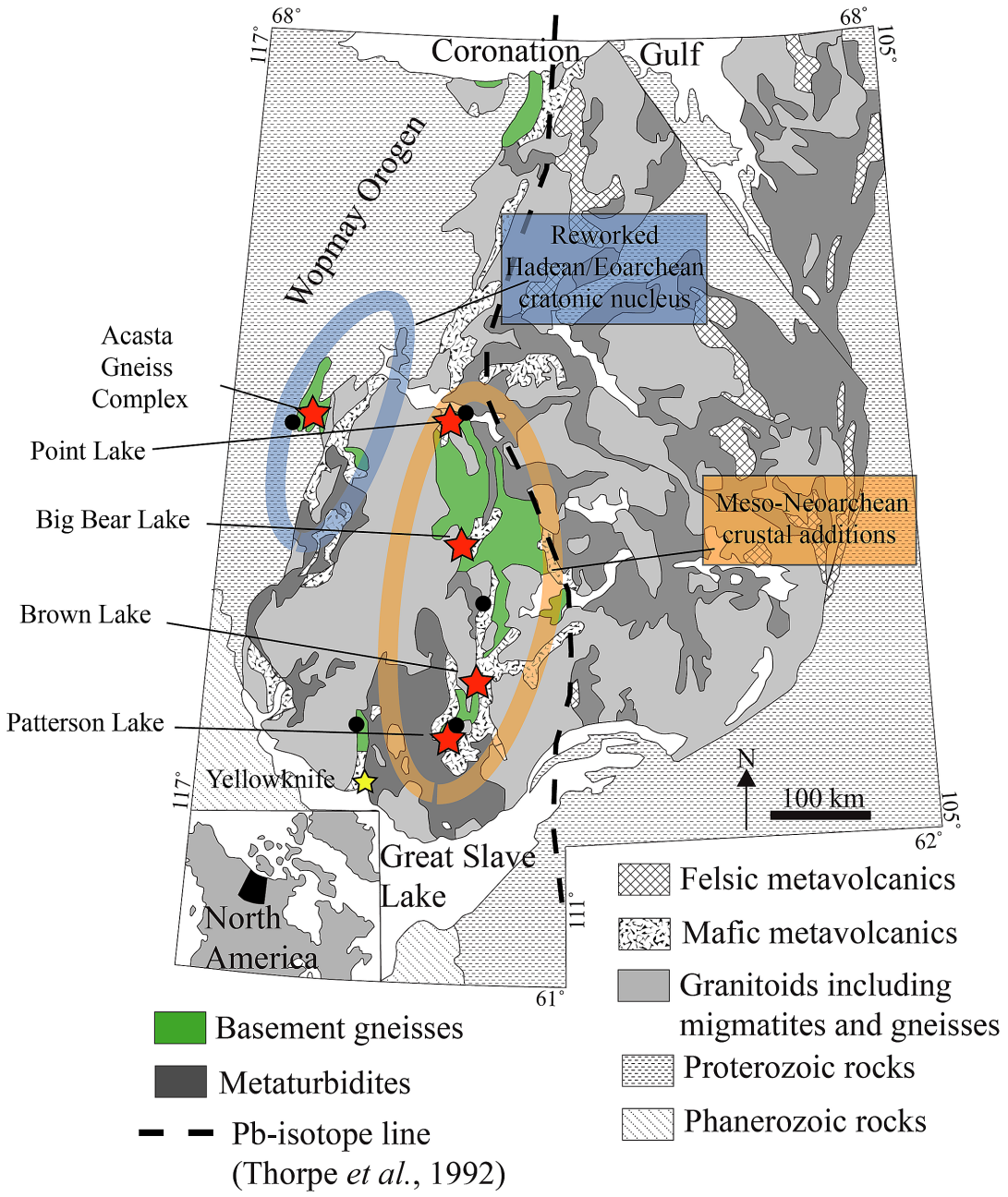

Figure 1 Geologic map of the Slave craton highlighting the major domains that contain basement gneisses. Map modified from St. Onge *et al.* (1988); Bleeker *et al.* (1999a,b). Major basement complexes are shown along with crustal province boundaries inferred from Nd and Pb isotope data (Davis and Hegner, 1992; Thorpe *et al.*, 1992). Red stars indicate key locations sampled in this study and coloured circles are locations where detrital zircons have been analysed for their U-Pb-Hf systematics as described in Figure 3 and the Supplementary Information.

rocks on Earth (*e.g.*, Bowring and Williams, 1999; Reimink *et al.*, 2016a). Recent petrologic and geochemical studies have documented systematic trends in the geochemical character of AGC rocks through time (*e.g.*, Reimink *et al.*, 2016b; 2018), which are used here to evaluate continued crustal growth in the broader Slave craton.

Previous work on the CSBC focused on preliminary field characterisation, geochronology, and its structural evolution (*e.g.*, Isachsen and Bowring, 1997; Bleeker *et al.*, 1999a,b; Ketchum *et al.*, 2004). Many of the exposed rocks in the CSBC are deformed, masking primary field relationships. Multiple magmatic pulses have been clearly defined within the Slave basement gneisses (van Breemen *et al.*, 1992; Bleeker *et al.*, 1999a; Sircombe *et al.*, 2001; Ketchum *et al.*, 2004), with major events from 4.02–2.8 Ga defined by Bleeker and Davis (1999) and summarised by Sircombe *et al.* (2001). Distinct magmatic pulses are evident at ~3.4–3.3 Ga, 3.26–3.2 Ga, 3.16–3.1 Ga, 3.06–3.01 Ga, 2.99–2.93 Ga, and 2.9–2.85 Ga. This nearly continuous record of magmatism makes the CSBC an excellent natural laboratory to study crust formation mechanisms over an important period of continent formation on Earth.

Results

Sample descriptions, whole rock compositions, and U-Pb-Hf data from individual analyses can be found in the Supplementary Information, along with intra-rock sample averages (*i.e.* averages from all magmatic zircons within a given sample) plotted in Figure 3.

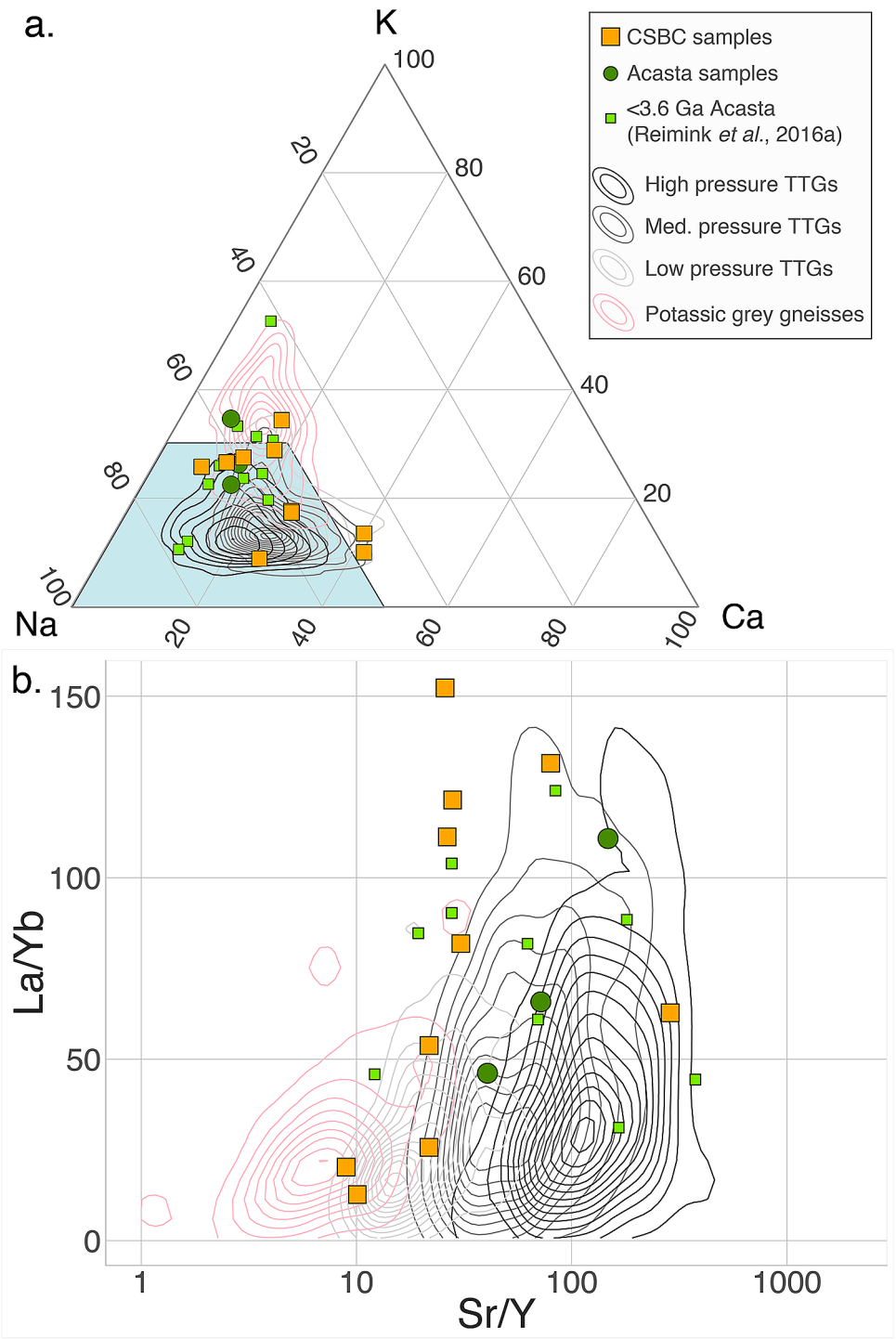

Figure 2 **(a)** Molar K-Na-Ca diagram. Orange squares are CSBC samples from this study. Green symbols are <3.6 Ga samples from the Acasta Gneiss Complex, small squares are samples measured by Reimink *et al.* (2016b) and dark green circles are samples added in this study. Contour density fields are high pressure TTGs (black), medium pressure TTGs (medium grey), low pressure TTGs (light grey), and potassic Archean grey gneisses (pink). Data used to construct these fields are taken from Moyen (2011). The blue field outlines sodic trondhjemites. **(b)** La/Yb *versus* Sr/Y for rocks from the Slave basement gneisses. Symbols as in **(a)**.

Juvenile Crustal Growth of the Slave Craton

Most of the rocks analysed here from the CSBC have elemental compositions similar to typical Archean grey gneiss suites (Moyen and Martin, 2012) and can be classified as TTGs (tonalite-trondhjemite-granodiorites). The sodic nature of these CSBC granitoids (Na_2O/K_2O generally >1.3) and relative enrichments in the incompatible trace elements suggests a derivation by partial melting of hydrated basalt (as summarised in Moyen, 2011; Moyen and Martin, 2012). The La/Yb and Sr/Y of sodic melts typically increase with more residual garnet and a greater depth of melting. CSBC rocks have a range in La/Yb and Sr/Y, but they fall within the range of Archean TTGs, typically comparable to the medium and high pressure TTGs (Fig. 2).

The Hf isotope data from AGC granitoid rocks are broadly similar to trends seen in previous Hf isotope studies of AGC zircons (*e.g.*, Iizuka *et al.*, 2009; Bauer *et al.*, 2017; Fig. 3). Notably, >3.6 Ga zircons from the AGC have significantly negative initial εHf values that fall along an evolution line suggestive of reworking of Hadean protocrust (*e.g.*, Bauer *et*

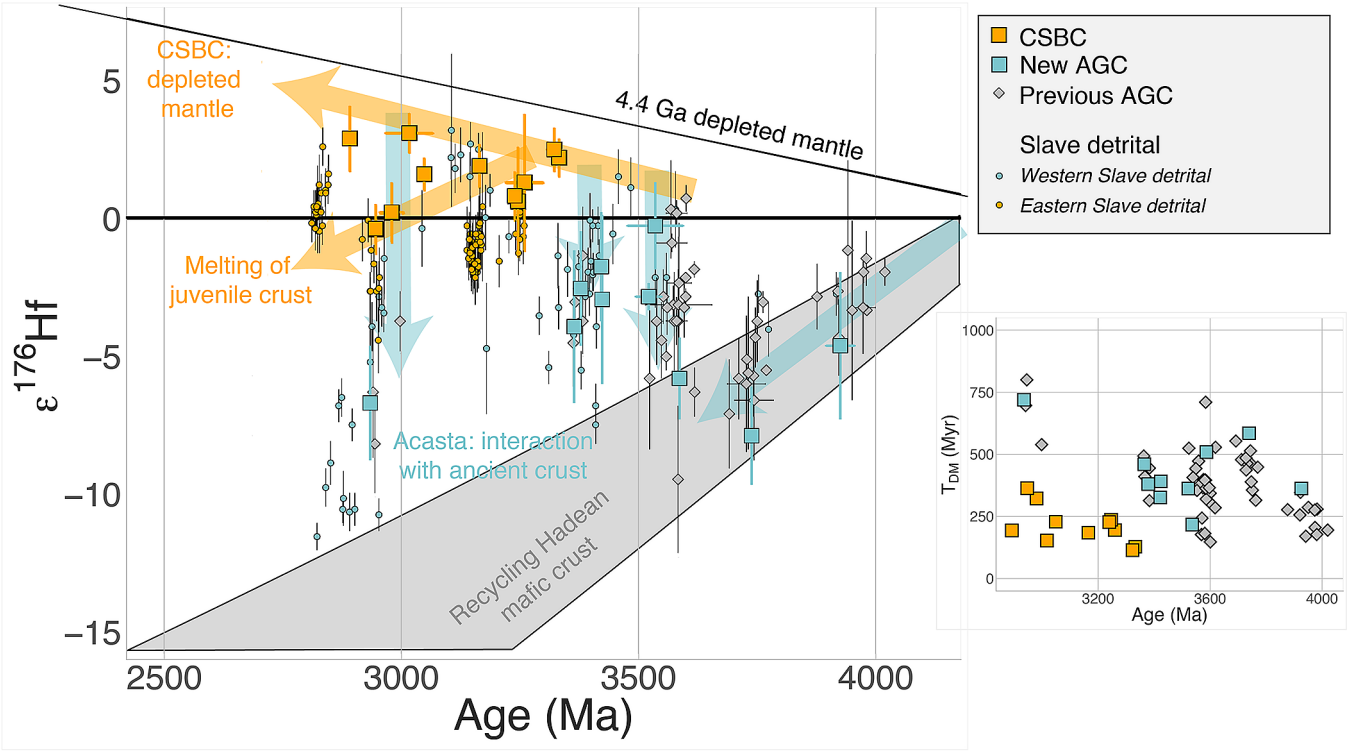

Figure 3 Zircon Hf isotope data from Slave basement gneisses. Orange symbols are analyses from the CSBC, blue are new analyses from the AGC, grey diamonds are a compilation of Acasta Hf isotope data (sources in the text), and small circles are single detrital zircon analyses from sediments of the Slave Craton Cover Group sequence (Pietranik *et al.*, 2008). Note that detrital zircon analyses are grouped by sediment location (see Supplementary Information). Grey field is the evolution of Hadean mafic protocrust, while orange and blue lines show our interpretations (sloped lines for time-integrated isotope evolution, vertical lines for mixing) for systematic petrogenetic differences between the two portions of the Slave basement gneisses. The Archean depleted mantle evolution line shown here is the connector line between a chondritic source at 4.4 Ga and modern MORB εHf values of +17. Calculated with respect to this model evolution for the depleted mantle, the inset shows the maximum crustal residence times (depleted mantle model ages calculated using a source $^{176}Lu/^{177}Hf$ of 0.015, and then subtracting the U-Pb crystallisation age from this model age) for all Slave craton Hf isotope data. The transition from long to short crustal residence times occurs at 3.6 Ga.

al., 2017). In contrast, younger AGC granitoids that formed between 2.95 and 3.6 Ga have higher εHf that is clearly offset from the Hadean protocrust reworking trend (Fig. 3) suggesting that these new crustal additions involved mixing between recently-mantle-derived crustal magmas and Hadean protocrust. Magmatic assimilation of ancient crust is the preferred mechanism for isotopic mixing in this case, supported by the presence of >3.6 Ga xenocrystic zircons found in 3.6 Ga magmatic rocks (*e.g.*, Iizuka *et al.*, 2007; Reimink *et al.*, 2016a).

The CSBC represents the major volume of the preserved Slave cratonic nucleus. Zircons from CSBC granitoids have positive initial εHf values, distinct from AGC rocks of similar age, indicating derivation from a source that evolved with higher-than-chondritic Lu/Hf. Our Hf isotope data suggest that these CSBC granitoids represent largely new crustal additions from the mantle and did not interact with >3.6 Ga material to any significant extent. We interpret negative εHf values within the CSBC to be due to internal reworking of older (*ca.* 3.35 Ga) silicic material, however, there is no indication within the CSBC data that much older, AGC-aged rocks, were present in that area. This differs significantly from the original interpretation of a previous study (Pietranik *et al.*, 2008) that used detrital zircons from the sedimentary sequence deposited directly on the CSBC rocks. These detrital zircon grain U-Pb-Hf data were grouped from across the entire craton, lumping terranes together to infer episodic mafic crust extraction and protracted reworking (Pietranik *et al.*, 2008). However, when the detrital zircon data are subdivided by terranes, the U-Pb-Hf data from these grains matches our new data well, supporting our interpretations (Figs. 3, S-1).

Isotopic Structure of the Slave Craton and the Transition to Short-lived Protocrust

The new AGC data are consistent with a previous model suggesting that >3.7 Ga rocks in the AGC were derived by melting of long-lived Hadean protocrust (*e.g.*, Iizuka *et al.*, 2009; Guitreau *et al.*, 2014; Bauer *et al.*, 2017; Reimink *et al.*, 2018), which has been documented in several other ancient gneiss localities (*e.g.*, Kemp *et al.*, 2010; O'Neil *et al.*, 2013). Rocks of the AGC that were produced from melts of this protocrust have major element compositions representative of shallow-level differentiation, both by fractional crystallisation and shallow-level melting (*e.g.*, Reimink *et al.*, 2014, 2016a,b, 2018). In contrast, the positive initial εHf values in the CSBC show that this geographically dominant swath of evolved crust was not derived by the remelting of long-lived Hadean mafic crust. Instead, the vast majority of the pre-2.9 Ga Slave craton was progressively, and rapidly, derived from mantle sources throughout the Mesoarchean without significant interaction with older crust. What isotopic variation is present can be easily explained by a small amount of assimilation of the older generation of CSBC crust (*ca.* 3.3–3.4 Ga).

Prevailing models for Archean TTG petrogenesis (*e.g.*, Moyen and Martin, 2012) dictate that rocks of these compositions were not direct mantle melts but instead formed by partial melting of mantle-derived basalts, thus requiring some, albeit short, intervening crustal residence history in the isotopic evolution from their mantle source. Maximum crustal residence times can be estimated by calculating the difference between the age of the rock and the depleted mantle model ages for the Hf isotope data (using an average Lu/Hf ratio for

mafic crust and a model depleted reservoir). These residence times depend on the assumed Hf isotope evolution of both the crustal precursor and the depleted mantle, so they should be considered relative values rather than absolute time intervals. Nevertheless, the relatively brief protocrustal residence prior to melting to produce the CSBC TTGs is distinctly different from the >400 Myr protocrustal residence times documented in several Hadean-Eoarchean crustal blocks described above, including the AGC (Fig. 3, inset). The relatively rapid reworking of mafic protocrust in the CSBC is similar to that seen in parts of many Neoarchean terranes and the modern plate tectonics dominated Earth.

Implications for Craton Formation Mechanisms

Magmatic events occurred in both the CSBC and the AGC during similar times (3.4–3.3 Ga and 2.95 Ga), and produced rocks with similar elemental compositions (Fig. 2). The Hf isotope distinction between these two crustal blocks, where rocks from the CSBC have higher initial εHf values than their AGC counterparts (Fig. 3), is important for evaluating crustal production mechanisms. In the AGC area, Hadean-Eoarchean crust was involved in the formation of Mesoarchean granitoids whereas CSBC rocks were mostly derived from newly formed sources whose isotopic compositions were similar to some models for Archean depleted mantle compositions (*i.e.* positive εHf values).

Several Archean granite-greenstone terranes appear to have been generated by some form of so-called 'vertical tectonics' either by a density inversion formed by erupted mafic rocks lying on top of partially molten, granitic, mid-crust (*e.g.*, Collins *et al.*, 1998), or by melting at the base of a thickened oceanic plateau (*e.g.*, Smithies *et al.*, 2003). When mafic rocks are erupted through pre-existing continental rocks, as in the gravitational instability model, there is typically a significant amount of crustal assimilation and the mafic rocks record this in their isotopic systematics. Yet, the CSBC felsic rocks that were produced over a ~500 Myr interval show initial Hf isotopic compositions paralleling the isotopic evolution of a modelled depleted mantle that began forming at 4.4 Ga. Though the exact Hf isotope evolution of the depleted mantle is uncertain, there is no indication in the younger TTGs for involvement of significantly older crustal basement, either by long-term storage of mafic crust or by assimilation of pre-existing crustal sections in the CSBC. In contrast, crustal residence times recorded in areas where melting at the base of an oceanic plateau is invoked, such as the Pilbara craton, extend up to a billion years, and crust formed in this manner has depleted mantle model ages reflecting this ancient parentage (*e.g.*, Smithies *et al.*, 2003). This feature is notably absent in all of the CSBC Hf isotope dataset.

The isotopic differences and spatial extent of newly created crustal rocks between the CSBC and AGC areas are similar to those found in modern plate margin provinces where new crust is being created adjacent to, but spatially distinct from, older continental crust. On the modern Earth, major zones of continental growth occur at the edge of pre-existing continental crust. When subduction zones are developed along continental margins, the new magmas produced in these settings often show isotopic signatures that systematically vary from primitive mantle-like near the subduction zone to more isotopically evolved compositions toward the continental mass (*e.g.*, the $^{87}Sr/^{86}Sr$ = 0.706 line in the Western US; Kistler and Peterman, 1973). Indeed, the CSBC rocks have trace element compositions compatible with a subduction zone (*e.g.*, enrichment in large-ion lithophile elements and depletion in high field strength elements; Fig. S-2), and such signatures have been used to argue for evidence of plate margin settings in the Archean, though this is far from resolved (*e.g.*, Moyen *et al.*, 2012). In fact, this subduction-accretion process was invoked to explain isotopic trends in ~2.6 Ga granites in the Slave craton (Davis and Hegner, 1992) that mimic the trends of the 3.4–2.9 Ga Slave craton gneisses.

By 3.7 Ga, the Acasta area had stabilised as an evolved continental nucleus produced by reprocessing of Hadean-aged protocrust (*e.g.*, Reimink *et al.*, 2016b; 2018). At 3.55 Ga new crustal rocks were created in the AGC from a source containing juvenile, mantle-derived input. The spectrum of initial εHf in these rocks is interpreted to be due to variable interaction between juvenile magmas and the rocks of the ancient continental nucleus *via* assimilation. This process clearly occurred as older zircons occur as xenocrysts in ~3.6 Ga samples. We also infer that assimilation generated the isotopic spread in the AGC at 3.4 and 2.95 Ga. During this same time, the majority of the CSBC crust was being constructed entirely from mantle sources, *i.e.* sources with no evidence of significant crustal prehistory. Because no substantially older crustal nucleus existed in the CSBC, the magmas that built this crust retained the depleted mantle isotopic signature. Furthermore, throughout this process, even the latest magmatic rocks were not assimilating and interacting with previously formed CSBC basement, suggesting lateral, rather than vertical, growth of the crust. Processes akin to modern subduction provide one mechanism to generate these isotopic and petrologic characteristics of the Slave basement gneisses, and indeed, models have suggested that subduction can initiate on the margins of plume-derived magmatic systems (*e.g.*, Geyra *et al.*, 2015). This is perhaps the mechanism that generated the 3.75–3.6 Ga transition in the AGC. Similar geodynamic changes have been invoked for other locations on Earth at different times (*e.g.*, Næraa *et al.*, 2012), suggesting that such transitions were not contemporaneous global changes, but occurred in different places at different times. Nevertheless, the CSBC represents a clear example of Mesoarchean crust that was formed by addition of new, juvenile, mass to the continent.

Acknowledgements

We thank Chiranjeeb Sarkar for assistance with the U-Pb-Hf analyses, Scott Cairns and the Northwest Territories Geological Survey office for field support, and Tom Chacko, Ann Bauer, and Josh Davies, for valuable discussions. We also thank Matt Scott and Michael Long for assistance in the field. Thoughtful reviews by Tony Kemp and one anonymous reviewer substantially improved this manuscript. We thank Helen Williams for editorial handling.

Editor: Helen Williams

Additional Information

Supplementary Information accompanies this letter at http://www.geochemicalperspectivesletters.org/article1907.

Cite this letter as: Reimink, J.R., Pearson, D.G., Shirey, S.B., Carlson, R.W., Ketchum, J.W.F. (2019) Onset of new, progressive crustal growth in the central Slave craton at 3.55 Ga. *Geochem. Persp. Let.* 10, 8–13.

References

Bauer, A.M., Fisher, C.M., Vervoort, J.D., Bowring, S.A. (2017) Coupled zircon Lu–Hf and U–Pb isotopic analyses of the oldest terrestrial crust, the >4.03 Ga Acasta Gneiss Complex. *Earth and Planetary Science Letters* 458, 37-48.

Bleeker, W., Davis, W.J. (1999) The 1991-1996 NATMAP Slave Province Project: Introduction. *Canadian Journal of Earth Sciences* 36, 1033-1042.

Bleeker, W., Ketchum, J.W., Davis, W.J. (1999a) The Central Slave Basement Complex, Part II: age and tectonic significance of high-strain zones along the basement-cover contact. *Canadian Journal of Earth Sciences* 36, 1111-1130

Bleeker, W., Ketchum, J.W., Jackson, V.A., Villeneuve, M.E. (1999b) The Central Slave Basement Complex, Part I: its structural topology and autochthonous cover. *Canadian Journal of Earth Sciences* 36, 1083-1109.

Bowring, S.A., Williams, I.S. (1999) Priscoan (4.00–4.03 Ga) orthogneisses from northwestern Canada. *Contributions to Mineralogy and Petrology* 134, 3-16.

Collins, W.J., Van Kranendonk, M.J., Teyssier, C. (1998) Partial convective overturn of Archaean crust in the east Pilbara Craton, Western Australia: driving mechanisms and tectonic implications. *Journal of Structural Geology* 20, 1405-1424.

Davis, W.J., Hegner, E. (1992) Neodymium isotopic evidence for the tectonic assembly of Late Archean crust in the Slave Province, northwest Canada. *Contributions to Mineralogy and Petrology* 111, 493-504.

Dhuime, B., Wuestefeld, A., Hawkesworth, C.J. (2015) Emergence of modern continental crust about 3 billion years ago. *Nature Geoscience* 8, 552-555.

Guitreau, M., Blichert-Toft, J., Mojzsis, S.J., Roth, A.S.G., Bourdon, B., Cates, N.L., Bleeker, W. (2014) Lu–Hf isotope systematics of the Hadean–Eoarchean Acasta Gneiss Complex (Northwest Territories, Canada). *Geochimica et Cosmochimica Acta* 135, 251-269.

Iizuka, T., Komiya, T., Ueno, Y., Katayama, I., Uehara, Y., Maruyama, S., Hirata, T., Johnson, S.P., Dunkley, D.J. (2007) Geology and zircon geochronology of the Acasta Gneiss Complex, northwestern Canada: New constraints on its tectonothermal history. *Precambrian Research* 153, 179–208, doi: 10.1016/j.precamres.2006.11.017.

Iizuka, T., Komiya, T., Johnson, S.P., Kon, Y., Maruyama, S., Hirata, T. (2009) Reworking of Hadean crust in the Acasta gneisses, northwestern Canada: Evidence from in-situ Lu–Hf isotope analysis of zircon. *Chemical Geology* 259, 230-239.

Isachsen, C.E., Bowring, S.A. (1997) The Bell Lake group and Anton Complex: a basement – cover sequence beneath the Archean Yellowknife greenstone belt revealed and implicated in greenstone belt formation. *Canadian Journal of Earth Sciences* 34, 169-189.

Kemp, A.I.S., Wilde, S.A., Hawkesworth, C.J., Coath, C.D., Nemchin, A., Pidgeon, R.T., Vervoort, J.D., DuFrane, S.A. (2010) Hadean crustal evolution revisited: New constraints from Pb–Hf isotope systematics of the Jack Hills zircons. *Earth and Planetary Science Letters* 296, 45-56.

Ketchum, J., Bleeker, W., Stern, R.A. (2004) Evolution of an Archean basement complex and its autochthonous cover, southern Slave Province, Canada. *Precambrian Research* 135, 149-176.

Kistler, R.W., Peterman, Z.E. (1973) Variations in Sr, Rb, K, Na, and Initial Sr87/Sr86 in Mesozoic Granitic Rocks and Intruded Wall Rocks in Central California. *Geological Society of America Bulletin* 84, 3489-3512.

Moyen, J.-F. (2011) The composite Archaean grey gneisses: Petrological significance, and evidence for a non-unique tectonic setting for Archaean crustal growth. *Lithos* 123, 21-36.

Moyen, J.-F., Martin, H. (2012) Forty years of TTG research. *Lithos* 148, 312-336.

Næraa, T., Scherstén, A., Rosing, M.T., Kemp, A.I.S., Hoffmann, J.E., Kokfelt, T.F., Whitehouse, M.J. (2012) Hafnium isotope evidence for a transition in the dynamics of continental growth 3.2 Gyr ago. *Nature* 485, 627-630.

O'Neil, J., Boyet, M., Carlson, R.W., Paquette, J.-L. (2013) Half a billion years of reworking of Hadean mafic crust to produce the Nuvvuagittuq Eoarchean felsic crust. *Earth and Planetary Science Letters* 379, 13-25.

Pietranik, A.B., Hawkesworth, C.J., Storey, C.D., Kemp, A.I.S., Sircombe, K.N., Whitehouse, M.J., Bleeker, W. (2008) Episodic, mafic crust formation from 4.5 to 2.8 Ga: New evidence from detrital zircons, Slave craton, Canada. *Geology* 36, 875-878.

Reimink, J.R., Chacko, T., Stern, R.A., Heaman, L.M. (2014) Earth's earliest evolved crust generated in an Iceland-like setting. *Nature Geoscience* 7 529-533.

Reimink, J.R., Chacko, T., Stern, R.A., Heaman, L.M. (2016a) The birth of a cratonic nucleus: lithogeochemical evolution of the 4.02–2.94 Ga Acasta Gneiss Complex. *Precambrian Research* 281, 453-472.

Reimink, J.R., Davies, J.H.F.L., Chacko, T., Stern, R.A., Heaman, L.M., Sarkar, C., Schaltegger, U., Creaser, R.A., Pearson, D.G. (2016b) No evidence for Hadean continental crust within Earth's oldest evolved rock unit. *Nature Geoscience* 9, 777-780.

Reimink, J.R., Chacko, T., Carlson, R.W., Shirey, S.B., Liu, J., Stern, R.A., Bauer, A.M., Pearson, D.G., Heaman, L.M. (2018) Petrogenesis and tectonics of the Acasta Gneiss Complex derived from integrated petrology and ^{142}Nd and ^{182}W extinct nuclide-geochemistry. *Earth and Planetary Science Letters* 494, 12-22.

Sircombe, K.N., Bleeker, W., Stern, R.A. (2001) Detrital zircon geochronology and grain-size analysis of a 2800 Ma Mesoarchean proto-cratonic cover succession, Slave Province, Canada. *Earth and Planetary Science Letters* 189, 207-220.

Smithies, R.H., Champion, D.C., Cassidy, K.F. (2003) Formation of Earth's early Archaean continental crust. *Precambrian Research* 127, 89-101.

St. Onge, M.R., King, J.E., Lalonde, A.E. (1988) Geology, East - Central Wopmay Orogen, District of Mackenzie, Northwest Territories. Geological Survey of Canada, Open File 1923. doi: 10.4095/130452.

Thorpe, R.I., Cumming, G.L., Mortensen, J.K. (1992) A Significant Pb Isotope Boundary in the Slave Province and Its Probable Relation To Ancient Basement in the western Slave Province. Geological Survey of Canada, Open File 2484, 179-184, doi:10.4095/133349.

van Breemen, O., Davis, W.J., King, J.E. (1992) Temporal distribution of granitoid plutonic rocks in the Archean Slave Province, northwest Canadian Shield. *Canadian Journal of Earth Sciences* 29, 2186-2199.

Geochemical Perspectives Letters

Onset of new, progressive crustal growth in the central Slave craton at 3.55 Ga

J.R. Reimink, D.G. Pearson, S.B. Shirey, R.W. Carlson, J.W.F. Ketchum

Supplementary Information

The Supplementary Information includes:

- Elemental Compositions
- Ages and Zircon Characteristics
- Comparison and Reinterpretation of Previous Detrital Zircon Data
- Hafnium-isotope Data from the AGC
- Sample Descriptions and Methods
- Sample Descriptions
- Sample Preparation
- LA-ICPMS Methods
- Data Reduction Notes
- U-Pb-Hf Isotope Summary for Each Sample
- Supplemental Methods Regarding U-Pb-Hf Isotope Data Treatment
- Tables S-1 and S-2
- Figures S-1 to S-4
- Supplementary Information References

Elemental Compositions

These samples span a wide range of major element compositions, with SiO_2 ranging from 58–77 wt. %. The majority have high Na_2O/K_2O, from 0.9–4.5. In general, the CSBC granitoids analysed here are mostly trondhjemites (Fig. 1), though some samples have higher CaO or K_2O contents than typical Archean TTGs (tonalite-trondhjemite-granodiorite). The three samples analysed in this study from Acasta (JR16-101;102;103) are all similar to previously documented <3.6 Ga granitoids in the AGC (Reimink *et al.*, 2016a), and nearly identical to a ~3.4 Ga sample documented in that work (JR13-802).

The CSBC rocks have trace-element patterns typical of Archean TTGs with enrichments in the large-ion-lithophile elements (Rb, U, Th), depletions in Nb and Ta, as well as Pb enrichments. There are highly variable REE contents among samples in this suite, with La/Yb ranging from 12–152. Both positive and negative Eu-anomalies are present, although several have no Eu anomaly.

Ages and Zircon Characteristics

Both CSBC and AGC samples analysed here have ages that correspond to the major magmatic pulses discussed in the main text, including the 3.4–3.3 Ga, and 2.95 Ga events. Several CSBC samples contain xenocrystic zircon cores representing crustal recycling in some form, either by inheritance from their sources during partial melting, or by assimilation of country rock into the magma upon emplacement. No xenocrystic cores were found to be older than 3.4 Ga. Several magmatic events within the CSBC and AGC have nearly identical ages which argues for the proximity of these crustal blocks to each other. These events are ~3.3–3.4 Ga (Acasta samples JR16-102, 103, JR13-802 as well as samples documented by Bauer *et al.*, 2017; CSBC samples JR16-329, 333), and ~2.95 Ga (AGC samples JR13-304 and samples from Bauer *et al.*, 2017; CSBC samples JR16-512, 517, 519, 406). Zircon Hf-isotope compositions from CSBC granitoids are complex due to the polymetamorphic nature of these rocks and several samples contain multiple generations of magmatic zircon. For these samples we assigned ages and ε_{Hf} values to multiple populations after checking for Pb-loss using combined U-Pb-Hf systematics. No systematic geographical variations in ε_{Hf} are apparent within the CSBC dataset, though differences are seen between these rocks and those of the AGC.

Comparison and Reinterpretation of Previous Detrital Zircon Data

Pietranik *et al.* (2008) analysed 137 detrital zircons extracted from the sedimentary cover group that directly overlies the Central Slave Basement Complex samples (Sircombe *et al.*, 2001) for their Hf-isotope compositions. Using a combination of Hf- and O-isotope analyses, these authors concluded that the Slave craton basement gneiss complex was formed by episodic mafic crust extraction from the mantle, followed by extended reworking of this mafic crust. They suggested that zircons extracted from the Slave craton with $\delta^{18}O$ values indistinguishable from the mantle field had clear peaks in depleted-mantle Hf-extraction ages. Their conclusions are very different from our inference, based on igneous-sample derived zircon Hf-isotope data, that the bulk of the Slave craton basement gneisses were formed by progressive extraction from 3.55–2.9 Ga. In an attempt to rectify these two interpretations, we plot the detrital zircon Hf-isotope data by location, and compare to our inferences that the AGC and CSBC have distinctly different Hf-isotope signatures.

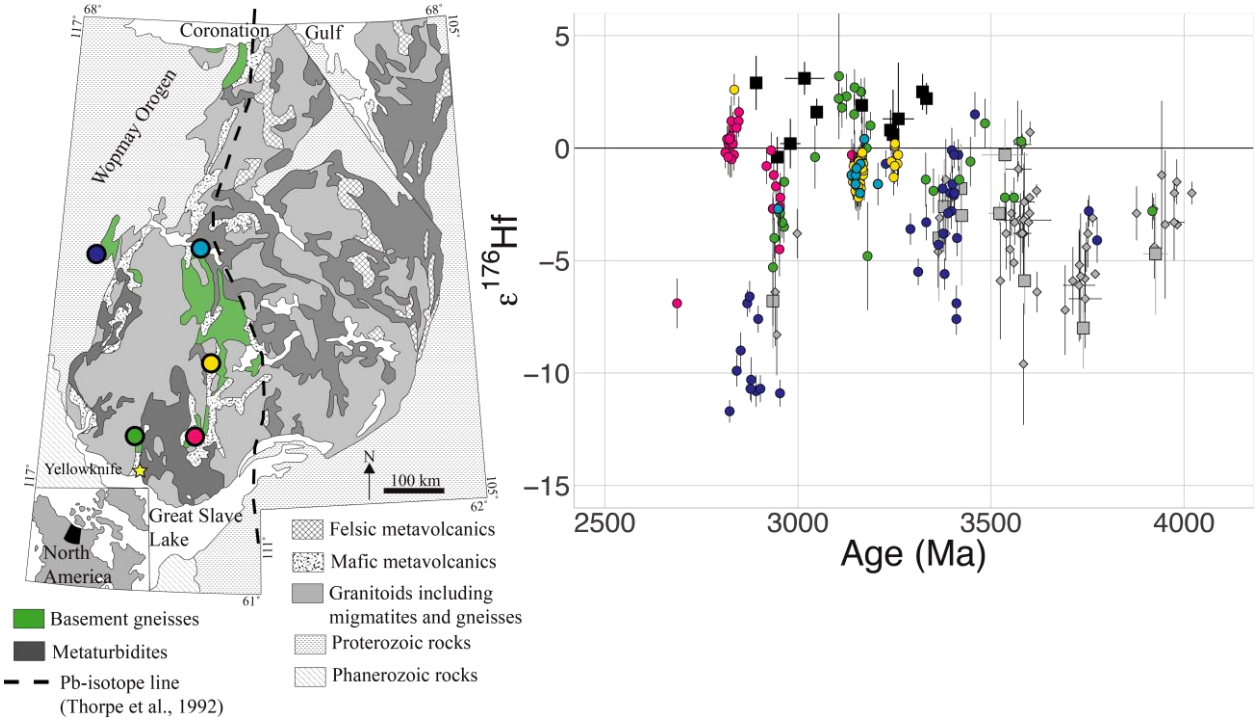

Figure S-1 Detrital zircon U-Pb-Hf isotope data from Pietranik *et al.* (2008) compared to our data from magmatic rocks. Grey symbols are from Acasta (diamonds from the compilation described in the main text, squares from the new data presented here). Black squares are the CSBC data presented in this work. Circles are detrital zircon data coloured by location, as on the map on the left. The green and purple locations (Exmouth Lake and Dwyer Lake, respectively) are grouped as "Western Slave detrital" in Figure 3 of the main text, while the pink, yellow, and light blue locations (Patterson, Loop, and Point Lakes, respectively) are grouped as "Eastern Slave detrital".

Here, as in Figure 3, colours correspond to detrital zircon sample location, except we have broken up the five sample locations into five groups. The grey symbols correspond to the same Acasta samples as in Figure 3, while the black squares are the CSBC data. Coloured circles are the detrital zircon data from Petranik *et al.* (2008), coloured by sample locations identified on the map. As in Figure 3, it is clear that all the >3.4 Ga grains, and nearly all grains with εHf values <-5 are restricted to the westernmost sample locations. One sample, Exmouth Lake (dark blue), sits directly on the AGC, and another, Dwyer Lake (green symbol) is from an area that is known to contain isotopic signatures indicative of the presence of AGC-aged crust (*e.g.*, Thorpe, 1992; Yamashita *et al.*, 1999). As the sediments deposited on the basement gneisses are interpreted to be rift-related sediments, they likely include detrital zircons from local sources (*e.g.*, Bleeker *et al.*, 1999; Sircombe *et al.*, 2001), and therefore are not representative of the broader Slave craton evolution. Our new basement gneiss data, when combined with a sample-by-sample analyses of the age-εHf relationships in the detrital zircon dataset, seems to validate this interpretation.

Our basement gneiss data suggests progressive tapping of a depleted mantle source (or close to the depeleted mantle composition) from 3.55 Ga onwards (Fig. 3) and our interpretation for the low εHf values in AGC rocks that are 3.4 and 2.95 Ga (-3 and -7, respectively) posits that juvenile depleted mantle material was simply mixing (via assimilation) with ancient, evolved, felsic crust. Older xenocrystic zircons in 3.4 Ga AGC rocks is further evidence for this process occurring. When the detrital zircon data is broken up by sediment location (Figs. 3 and S-1), the geographical similarities between CSBC and CSBC-derived sediments in age-εHf space, and similarities between AGC and AGC-derived sediments in the same space, imply that the regional differences seen in our igneous-sample based Hf data are robust.

Hafnium-isotope Data from the AGC

A substantial amount of Hf-isotope data has been collected from the AGC so far, summarised in some detail by Bauer *et al.* (2017), we provide the full list of references here: Amelin *et al.*, 1999; Amelin *et al.*, 2000; Bauer *et al.*, 2017; Guitreau *et al.*, 2012; Guitreau *et al.*, 2014; Iizuka and Hirata, 2005; Iizuka *et al.*, 2009; Reimink *et al.*, 2016b.

Sample Descriptions and Methods

During the summer of 2016 we collected several dozen samples of orthogneiss from the AGC and CSBC, in areas highlighted in Figure 1. Samples were selected for further analysis based on relative lithological homogeneity, lack of clear alteration products such as epidote veining and seriticisation, and preservation of igneous zircon. A subset of samples was processed for bulk geochemistry and zircon separation. Zircon from these samples were analysed by split-stream LA-ICPMS (LASS) methods at the University of Alberta in January of 2018 following the methods described in Reimink *et al.* (2016b). Zircons from seven samples described by Reimink *et al.* (2016a) were analysed in June of 2015 using identical LASS methods.

Sample Preparation

Samples were initially processed by slabbing 0.5–1.5 kg of hand sample, removing areas with obvious weathering or alteration, breaking slabs with a hammer, and crushing in an alumina jaw crusher. An aliquot of sample chips was sent to Washington State University's Geoanalytical Laboratory and crushed for elemental analysis using XRF and ICPMS.

Sample Descriptions

For descriptions of most of the Acasta samples analysed here, see Reimink *et al.* (2016a).

Samples from Acasta, ~10km SW of the discovery area

JR16-101

This sample comes from a large body of homogeneous, pink-coloured, foliated granodiorite containing mainly quartz, feldspar, and biotite. Veins of potassium feldspar and quartz cross-cut the outcrops, but within each outcrop the rock is a homogenous granodiorite, on the scale of tens of metres.

JR16-102

This sample is from a large body of homogeneous, pink-white, foliated granodiorite that has slightly more biotite than the previous sample. Outcrops have some epidote veining, though it is not pervasive. Rock contains mainly quartz, feldspar, and biotite.

JR16-103

This sample comes from a smaller body (~10 metres) of white granite that is near the sample locations described above (see GPS coordinates). This granite contains abundant quartz, feldspar, and biotite.

Samples from the Point Lake area in the CSBC

JR16-213

This sample is from a small, ~10 cm-wide, layer of banded gneiss that had been previously sampled by John Ketchum. This particular sample is a layer of darker tonalite, containing quartz, plagioclase, and a high proportion of biotite and amphibole. The gneissic fabric in this rock is defined by quartz-rich layers alternating with more leucocratic layers at the cm-scale.

JR16-215

Sample of a homogenous, foliated, quartz-diorite. This unit is cross-cut by coarse quartz-feldspar pegmatites across much of the outcrop. The sample of the quartz diorite contains a high proportion of amphibole and biotite, as well as plagioclase and quartz.

JR16-217

Sample of a fine-grained, light grey tonalite containing amphibole, plagioclase, biotite, and quartz and is associated with the quartz diorite sampled in JR16-215. Both of these samples are foliated and cross-cut by pegmatites.

JR16-236

This is a sample of the more evolved phase in the Augustus Granitoid complex. As such, it is coarse grained and heavily altered, containing abundant calcite, chlorite, and epidote-group minerals. The main portion of the rock is made up of quartz and plagioclase, with amphibole and biotite that have been altered to biotite and chlorite. The calcite and epidote occurs within veins and the plagioclase has been heavily sericitised.

JR16-254

This sample is a fine-grained granodiorite containing a small proportion of biotite and amphibole, with abundant plagioclase and quartz. Titanite is a common accessory mineral. Grain boundaries are mostly metamorphic and the sample has likely undergone significant grain-size reduction due to strain.

Samples from the Big Bear Lake area in the CSBC

JR16-328

This is a sample from coarse-grained tonalitic component to the basement gneisses. It is a foliated tonalite containing a small amount of amphibole, a high proportion of biotite and a majority of quartz and feldspar.

JR16-329

This sample is a granitic gneiss with a medium grain size. It contains very little alteration although many of the feldspars are sericitised. The major minerals are biotite, plagioclase, alkali -feldspar, and quartz, while titanite and apatite are common accessory minerals.

JR16-333

This sample is a medium-grained tonalite that contains a high proportion of amphibole and biotite. Other rock-forming

minerals are plagioclase and quartz, while titanite, apatite, unidentified oxides, and epidote make up accessory minerals. The epidote does not appear to be formed during alteration but occurs as discreet grains within the rock.

Sample from the Brown Lake area in the CSBC

JR16-406

This sample is a medium grained granite that contains biotite, plagioclase, quartz, and alkali feldspar. The biotite is occasionally altered to chlorite, while the feldspars have a moderate degree of sericitization.

Samples from the Patterson Lake area in the CSBC

JR16-512

This sample is a coarse-grained foliated tonalitic-granodioritic rock. It is foliated but not quite gneissic. Biotite content is variable across the outcrop though other aspects of the unit are consistent.

JR16-517

This sample consists of a foliated granite that contains large, potassium-feldspar phenocrysts. The sample also contains biotite, and quartz.

JR16-519

This sample is a medium-to-fine-grained granodiorite that contains biotite, quartz, minor plagioclase, and alkali feldspar as the major minerals. Titanite, apatite, and minor amounts of secondary chlorite make up the obvious accessory minerals. Some grains appear to be relict amphibole that have been altered to epidote and chlorite.

LA-ICPMS Methods

Twenty-two samples with identifiable zircon present in thin section were sent to ZirChron LLC for zircon separation using traditional methods (*e.g.*, magnetic separation, heavy liquids). Zircons returned from these analyses were mounted in epoxy, polished to mid-section and imaged using secondary-electron and backscatter-electron imaging on the Zeiss Auriga field emission SEM at the Carnegie Institution for Science. After imaging, samples were analysed by laser-ablation split-stream methods at the University of Alberta following the methods outlined in Reimink *et al.* (2016b) and summarised below.

Samples were ablated with a Resonetics Excimer 193 nm laser operating with a fluence of ~3 J/cm^2, a spot size of 33 μm, and a repetition rate of 8 Hz. U-Pb isotopic measurements were conducted on a Thermo Element-2XR mass spectrometer using a single secondary electron multiplier detector operating in peak hopping mode. Hafnium isotope compositions were made concurrently on a Thermo Neptune Plus mass spectrometer in multi-collector mode using multiple Faraday detectors fitted with 10^{11} amplifiers. Both U-Pb and Hf datasets were reduced using the Iolite software package in multiple mass spectrometer mode. Both standard and sample analyses were carefully filtered to only integrate sections of the analysis that had consistent U-Pb, Pb-Pb, and Hf-isotope compositions. Each analysis was given a qualitative score to evaluate the quality of the analysis, ranging from 1, meaning very consistent isotope ratios throughout the entire analysis time, to 4, meaning the data was so variable that no meaningful integrations could be used. Final data reduction and calculation of average compositions used only analyses with a 1–3 quality rating to avoid analyses with highly uncertain averages.

Both U-Pb and Hf isotope ratios were normalised to the Plesovice reference material as a primary standard, while zircon 91500, OG1, and in house standard LH91-15 were all monitored as secondary standards. The Yb-interference correction was monitored using MUN1, MUN3, and MUN4 synthetic zircons, each with distinct Yb/Hf ratios, and the apparent $^{173}Yb/^{176}Yb$ ratio was solved by iteratively changing this ratio in the Iolite reduction template such that MUN1, MUN3, and MUN4 zircon analyses returned the accepted $^{176}Hf/^{177}Hf$ ratio (0.282135; Fisher *et al.*, 2011). MUN3 and MUN4 zircon have much greater Yb/Hf than any unknown samples measured here.

All initial $^{176}Hf/^{177}Hf$ and $\varepsilon^{176}Hf$ values, and associated uncertainties, were fully propagated using the algorithms laid out in Ickert (2013). Our best estimate εHf values were calculated by assigning crystallisation ages to each sample. This age was calculated by taking the weighted mean $^{207}Pb/^{206}Pb$ age of the oldest consistent population of analyses, after removing inherited cores. This age was then used to calculate initial εHf values, and associated uncertainties, for all samples. Weighted mean εHf

values were then calculated from this population of analyses. Note that taking a weighted mean after calculating εHf values will ignore systematic uncertainties, however, the primary uncertainty in most of our weighted mean values comes from scatter within a population such that systematic uncertainties would add little extra uncertainty to these values.

One run, Run #4, had excess scatter on the measured Hf-isotope composition of the primary reference material (Plesovice). We interpret this to be due to oxide production within the plasma of the mass spectrometer, as the $^{173}Yb/^{176}Yb$ ratio needed to reproduce the true Hf-isotopic compositions of MUN zircons was different from those used during other sessions, and those commonly required to correct LASS Hf data on the UAlberta Neptune Plus instrument. However, the mean value for all standards during this session was equivalent to the accepted values. As we are using average values for unknown samples, taken from several analyses of co-magmatic zircons, this excess scatter on the standard samples does not affect our ultimate reported age and εHf values for samples run during this time (JR16-103; JR16-213; JR16-215).

Data Reduction Notes

All zircon analyses were rated on a scale of 1–4 based on a qualitative analysis of the quality of the run. These analyses were rated in a similar manner to Reimink *et al.* (2016b) and consisted of evaluating the consistency of measured U/Pb, $^{207}Pb/^{206}Pb$, Lu/Hf, and $^{176}Hf/^{177}Hf$ throughout an analysis. Below we lay out our criterion for ranking a given analysis with the scale of 1–4.

1. Nearly all of the time-resolved analysis had consistent U-Pb and Hf isotope compositions.
2. >50 % of the time-resolved analysis had consistent ages and Hf isotope compositions
3. <50 % of the time-resolved analysis had consistent ages and Hf isotope compositions, but some of the analysis was still consistent and useful
4. No portion of the time-resolved analysis was consistent. Not deemed to be useful information.

We only accepted analyses had analytical qualities that were <4. All data with raw $^{206}Pb/^{204}Pb$ ratios <500 and discordance <-40 were accepted. $^{207}Pb/^{206}Pb$ ages for each sample were calculated with the *weightedmean()* function in IsoplotR (Vermeesch, 2018), using the analyses with the oldest $^{207}Pb/^{206}Pb$ ages and their respective 2SE (propagated).

These 'best estimate' ages were then used to calculate εHf values for each sample. These εHf values were compared to εHf calculated at the $^{207}Pb/^{206}Pb$ age of the actual measurement, and used to evaluate intrinsic εHf variability.

Below, we describe the U-Pb-Hf isotope systematics for each sample, as well as the method used to calculate an age and εHf value for each sample. Uncertainties are calculated using the IsoplotR *weightedmean()* function and thus have two uncertainties reported. The first is the standard deviation and the second is the 95 % confidence interval (Vermeesch, 2018). Where no confidence interval is reported by the calculation, we have replaced with "NA".

U-Pb-Hf Isotope Summary for Each Sample

Acasta Gneiss Complex Samples

JR12-127

All 25 analyses were of acceptable consistency. The seven oldest analyses have consistent 7/6 ages and give a weighted mean age of 3587 ± 14/36 with an MSWD of 2.6. This age is in close agreement with the age determined by Reimink *et al.* (2016a) of 3582 ± 9 Ma, so we used the age determined here for Hf calculations. The weighted mean of the initial $^{176}Hf/^{177}Hf$ of the second through fifteenth analyses is 0.280338 ± 0.000019/0.000041 with an MSWD of 0.19. The weighted mean initial εHf value of the same population is -5.9 ± 0.7/1.5 with an MSWD of 0.43.

JR13-101

Twenty-three of 24 analyses were of acceptable consistency. The six oldest analyses have consistent 7/6 ages and give a weighted mean age of 3684 ± 10/27 with an MSWD of 0.22. This age is significantly younger than the age determined by Reimink *et al.* (2016a) for this sample, 3739 ± 6 Ma, determined by the weighted mean of 18 oldest analyses. We interpret the age of 3739 to be more accurate and therefore used this age to calculate initial Hf values. The weighted mean of the initial $^{176}Hf/^{177}Hf$ from all analyses is 0.280195 ± 0.000019/0.000040 with an MSWD of 0.27. The weighted mean initial εHf value from the oldest 18 analyses is -8 ± 0.9/1.8 with an MSWD of 0.32.

JR13-206

Twelve of 15 analyses were of acceptable consistency. The two oldest analyses have consistent 7/6 ages and give a weighted mean age of 3859 ± 24/NA with an MSWD of 0.054. This age is again significantly younger than the age determined by Reimink *et al.* (2016a) of 3926 ± 30. We used the latter age for Hf calculations as that age came from a weighted mean of the eight oldest ages, as opposed to the two use here. The weighted mean of the initial $^{176}Hf/^{177}Hf$ of the oldest two analyses is 0.280142 ± 0.000072/NA with an MSWD of 0.27. The weighted mean initial εHf value of the same population is -4.7 ± 2.7/NA with an MSWD of 0.31.

JR13-208

Twenty-three of 25 analyses were of acceptable consistency. The nine oldest analyses have consistent 7/6 ages and give a weighted mean age of 3522 ± 12/27 with an MSWD of 0.19. This age is slightly younger than the age determined by Reimink *et al.* (2016), which is 3573 ± 11 Ma, so we used the latter age for calculations. The weighted mean of the initial $^{176}Hf/^{177}Hf$ is 0.280415 ± 0.000022/0.000025 with an MSWD of 0.12 and one outlier rejected. This translates to an initial εHf value of -2.9 ± 0.5 at 3573 Ma.

JR13-304

Twenty-five of 25 analyses were of acceptable consistency. The nine oldest analyses have consistent 7/6 ages and give a weighted mean age of 2931 ± 13/30 with an MSWD of 0.38. This age agrees well with the previously determined age of 2935 ± 9 Ma. The weighted mean of the initial $^{176}Hf/^{177}Hf$ is 0.280705 ± 0.000022/0.000051 with an MSWD of 0.23 and no outliers rejected. This translates to an initial εHf value of -6.8 ± 0.9/2.1 at 2935 Ma.

JR13-802

Twenty-five of 25 analyses were of acceptable consistency. Two analyses had much older ages than the bulk of the igneous population and are interpreted to be xenocrystic cores. The third-thru-seventh oldest analyses have consistent 7/6 ages and give a weighted mean age of 3357 ± 16/52 with an MSWD of 0.65. This age is in good agreement with the previously determined age of this sample (3365 ± 13 Ma), which we use for the Hf-isotope calculations. The weighted mean of the initial $^{176}Hf/^{177}Hf$ is 0.280505 ± 0.000022/0.00007 with an MSWD of 1.4 and zero outliers rejected. This translates to an initial εHf value of -4.0 ± 0.9/2.8 at 3365 Ma with an MSWD of 1.

JR16-101

Eleven out of 19 analyses were of acceptable consistency. The five oldest analyses have consistent 7/6 ages and give a weighted mean age of 3536 ± 14/58.6 with an MSWD of 5.5. The next 6 analyses have 7/6 ages that yield a weighted mean 7/6 age of 3379.1 ± 5.4/15 with an MSWD of 1. The weighted mean initial εHf value of the oldest four analyses (calculated at the measured 7/6 age) of -2.3 ± 0.8/3.3 with an MSWD of 0.7. The weighted mean initial εHf of the next group of analyses is -2.6 ± 0.66/2.1 with an MSWD of 0.41. One outlier was rejected, as it is likely a metamorphic grain, having the same $^{176}Hf/^{177}Hf$ as the older magmatic suite of samples. These Hf-isotope values were calculated using the 7/6 age of the individual analysis.

JR16-102

Twenty-one out of 22 analyses were of acceptable consistency. The sample with the oldest 7/6 age is not obviously an inherited core. The second oldest analysis is not clearly different from other samples with younger 7/6 ages. A weighted mean of analyses 3–9 (in order of 7/6 age) gives an age of 3423.8 ± 5.6/14 with an MSWD of 1.4. A regression has an upper intercept age of 3407 ± 19/39. A weighted mean of the 4–10 oldest analyses gives and initial εHf value of -2.8 ± 1.3/3.3 with an MSWD of 4.7. We treat this as the best estimate of the initial Hf isotope composition of this sample, by removing the grains we interpret to be inherited, and analyses representing Pb-loss from inherited grains.

JR16-103

Twenty-one out of 26 analyses were of acceptable consistency. The oldest analysis had an anomalously old age, though it isn't clearly from a different growth zone. A weighted mean of analyses 4-10 gives an age of 3422.5 ± 4.6/12 Ma with an MSWD of 0.86. A regression through all the data (using option #4 in the *Concordia()* function gives an upper intercept age of 3442.4 ± 5.8/12. The weighted mean initial εHf value of the 4–10 oldest analyses is -0.2 ± 0.9/2.3 with an MSWD of 2.6.

Central Slave Basement Complex Samples

JR16-213

Twenty-eight out of 40 analyses were of acceptable consistency. No obvious cores were found in these samples. The two oldest analyses are from one single grain and may not represent the true age. Therefore, we took a weighted mean of the next four oldest analyses, with an age of 3260 ± 9.1/39.1 Ma and an MSWD of 4.2. The weighted mean initial εHf value of the 3–10 oldest analyses is 1.3 ± 1/2.5 with an MSWD of 1.5.

JR16-215

All 27 analyses were of acceptable consistency. The regression of all data gives an upper intercept age of 2678.4 ± 4.8/9.8. A weighted mean of the 310 analyses gives an age of 2706.2 ± 3.3/7.7 Ma with an MSWD of 0.45. The weighted mean initial εHf value of the oldest 3–13 analyses (with one analysis with low Hf excluded) is 3.7 ± 0.9/2 with an MSWD of 1.8. The low initial εHf value analyses are interpreted to be due to Pb-loss from inherited cores.

JR16-217

All 19 analyses were of acceptable consistency. U-Pb data shows very little scatter, though uncertainties are large, with one analysis having a younger 7/6 age. A weighted mean the 37 analyses gives an age of 2719.1 ± 5.8/18 with an MSWD of 0.86. The weighted mean initial εHf value of the entire population is -1.1 ± 0.5/1 at 2719 Ma with an MSWD of 0.47.

JR16-236

Six out of ten analyses were of acceptable consistency, the weighted mean 7/6 age of all analyses is 3246.2 ± 5.2/14 with an MSWD of 1.1, consistent with ID-TIMS data from other samples of this unit (Ketchum *et al.* unpublished data). The weighted mean initial εHf value of the entire population is 0.6 ± 0.7/2 at 3246.2 Ma with an MSWD of 0.19.

JR16-254

Twenty-two out of 23 analyses were accepted. They fall on a well-defined discordia line, with an upper intercept age of 3165 ± 2.4/4.9. This is slightly older than the weighted mean 7/6 age of the oldest 14 analyses, which is 3136.7 ± 4.9/11 with an MSWD of 0.85. The weighted mean initial εHf value of the entire population is 1.9 ± 0.4/0.8 at 3165 Ma with an MSWD of 0.6.

JR16-328

Thirty analyses out of 33 were accepted. The upper intercept age is 3241.7 ± 2.6/5.3 Ma, matching well with the weighted mean 7/6 age of the oldest 14 analyses, 3239.7 ±2.8/6.1 with an MSWD of 1.1. The weighted mean initial εHf value of the entire population is 0.8 ± 0.4/0.9 at 3241 Ma with an MSWD of 0.37.

JR16-329

Twenty-seven out of 49 analyses were accepted. The upper intercept age is 3312.1 ± 7.5/15 Ma which agrees with the weighted mean 7/6 age of the oldest seven analyses, 3322.6 ± 6/15 Ma with an MSWD of 1.7. The weighted mean initial εHf value of the entire population is 2.5 ± 0.4/0.8 at 3322.6 Ma with an MSWD of 0.7. This is the within uncertainty of the weighted mean initial εHf of the oldest seven analyses (2.7 ± 0.8/2.1, MSWD = 0.74).

JR16-333

All 33 analyses were accepted. The upper intercept age is 3332.8 ± 5/10 Ma. This is slightly older than the weighted mean 7/6 age of the oldest 29 analyses which is 3314 ± 2.5/5.8 with an MSWD of 0.22. The weighted mean of initial εHf value of the entire population is 2.2 ± 0.3/0.7 at 3332 Ma with an MSWD of 0.24.

JR16-406

Twenty-six out of 36 analyses were accepted. The weighted mean 7/6 age of the 2–5 analyses is 2980.2 ± 7.8/25. This age excludes the oldest analysis as an outlier and has an MSWD of 2.2. A second population of analyses 10–17 have a weighted mean 7/6 age of 2891.6 ± 3.9/9.6 Ma with an MSWD of 0.88. These two populations are distinct in their Hf isotope compositions as well as

age. The weighted mean initial εHf at 2980 Ma of the oldest 2–14 analyses is 0.2 ± 0.5/1.1 with an MSWD of 0.7. The weighted mean initial εHf of the rest of the population, calculated at 2891 Ma, is 2.9 ± 0.6/1.2 with an MSWD of 1.5.

JR16-512

Seventeen out of 40 analyses were accepted. A regression of all data yields an upper intercept age of 2946.4 ± 3.6/7.6 Ma. One older analysis has an older 7/6 age and is likely an inherited core. The weighted mean 7/6 age of the oldest 29 analyses is 2927.8 ± 6.7/16 Ma with an MSWD of 2.1. The weighted mean initial εHf value of the entire dataset is -0.4 ± 0.4/0.9 at 2946.4 Ma with an MSWD of 0.41.

JR16-517

Thirty-four analyses out of 47 analyses were of sufficient consistency. The weighted mean 7/6 age of the oldest 6 analyses is 3017 ± 12/49.8 Ma (MSWD = 3.2), in good agreement with the upper intercept of the discordia array, which is 2996 ± 7/15 Ma. The weighted mean initial εHf value of the entire dataset is 3.1 ± 0.4/0.7 at 3017 Ma with an MSWD of 0.61.

JR16-519

Out of 41 analyses, 35 were of sufficient consistency for further evaluation. A weighted mean age of the oldest six analyses gives a 7/6 age of 2998 ± 10/28 Ma with an MSWD of 2.6. This fits well with the upper intercept regression of 3048.6 ± 2.3/4.8 Ma. The weighted mean initial εHf value of all the data points is 1.6 ± 0.3/0.6 at 3048.6 Ma with an MSWD of 1.2.

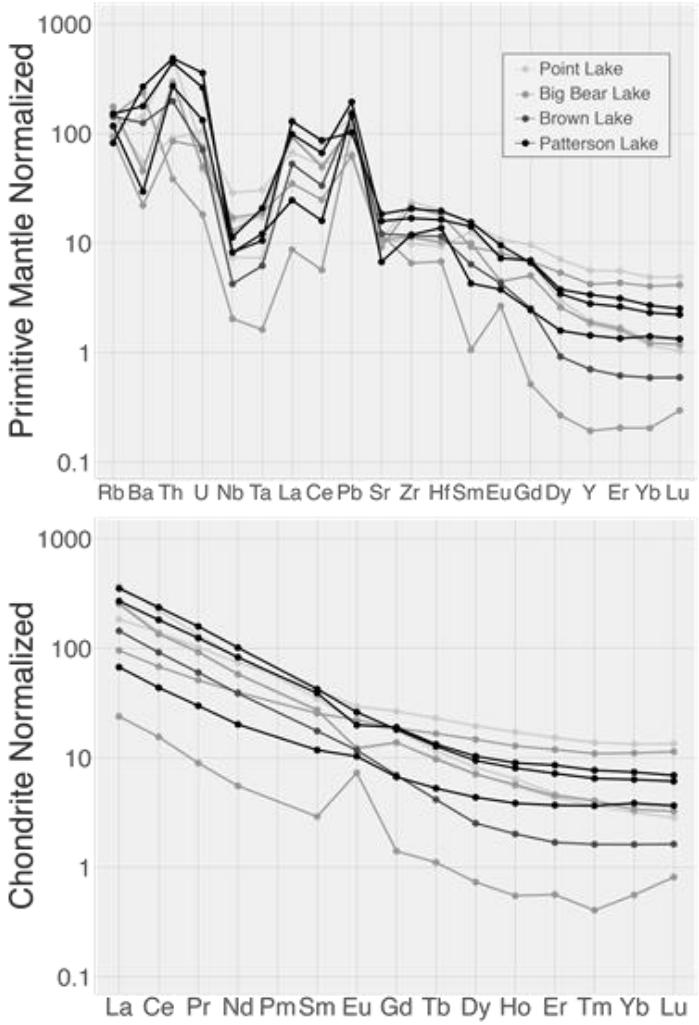

Figure S-2 Trace-element data from CSBC granitoids described here. Samples are divided by location and plotted normalised to primitive mantle (top) and chondrite (bottom) abundances.

Supplemental Methods Regarding U-Pb-Hf Isotope Data Treatment

Several studies have shown that spurious Hf-isotope data can be easily generated (*e.g.*, Amelin *et al.*, 2000; Kemp *et al.*, 2010; Vervoort and Kemp, 2016; and many others). Therefore, care must be taken when making age-εHf assignments to avoid biasing any dataset. Here, we investigated each sample carefully and assigned ages based on the $^{207}Pb/^{206}Pb$ ages, which are minimum age estimates. Below we show two samples as examples of how we approached data reduction.

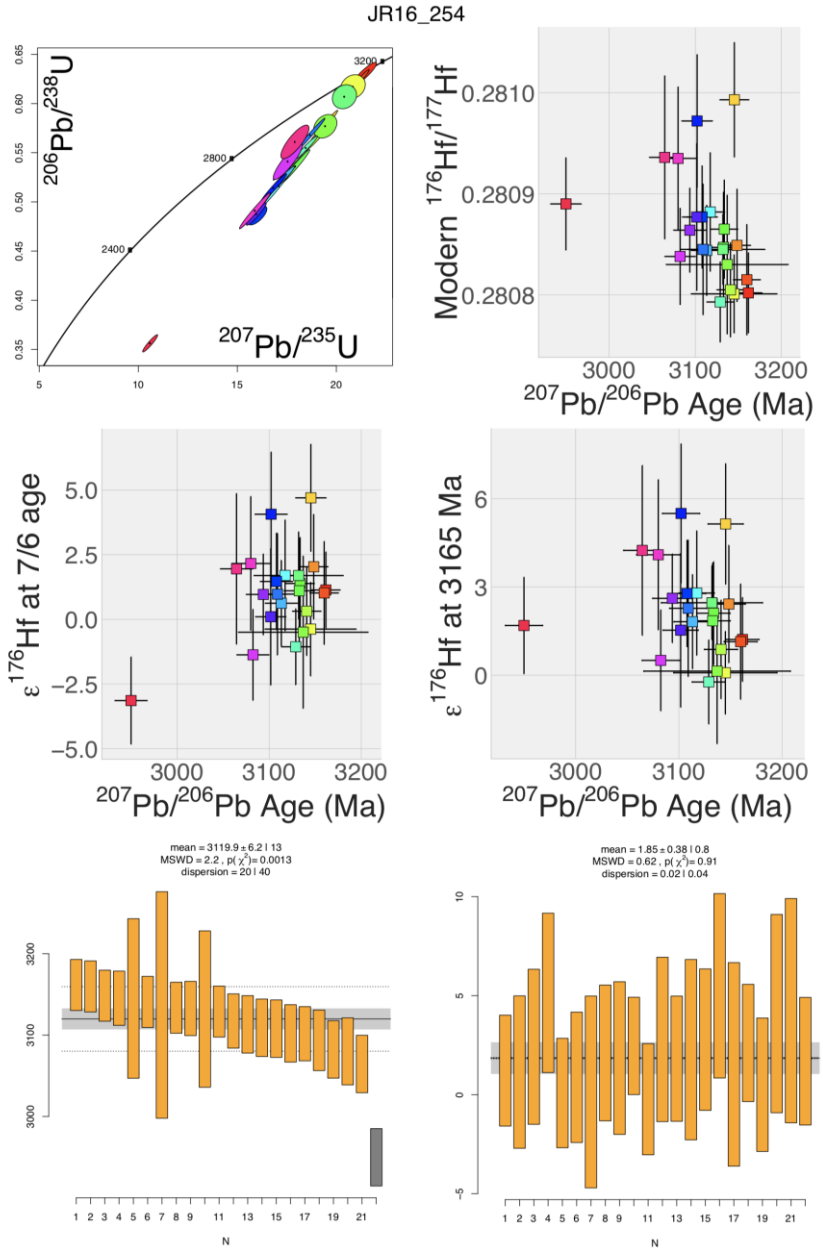

Figure S-3 Split stream U-Pb-Hf data from sample JR16-254. This sample shows relatively simple age-Hf isotope characteristics. The top four panes have individual analyses coloured by analysis number. The U-Pb systematics plot along a relatively simple discordia array. Though several analyses have radiogenic Hf-isotope compositions (high modern $^{176}Hf/^{177}Hf$), these analyses are often higher $^{176}Lu/^{17}Hf$ analyses and get ingrowth corrected down to lower initial values (compare top right with middle left). Correcting all Hf-isotope compositions back to a single age yields a simple εHf population (middle right) whereas when the samples are corrected to the $^{207}Pb/^{206}Pb$ age of the analysis, the εHf value is artificially low (middle left). The bottom two panes are the weighted mean calculations for the $^{207}Pb/^{206}Pb$ ages and εHf values calculated at the best age estimate for the sample (3165 Ma; upper intercept age of the discordia line).

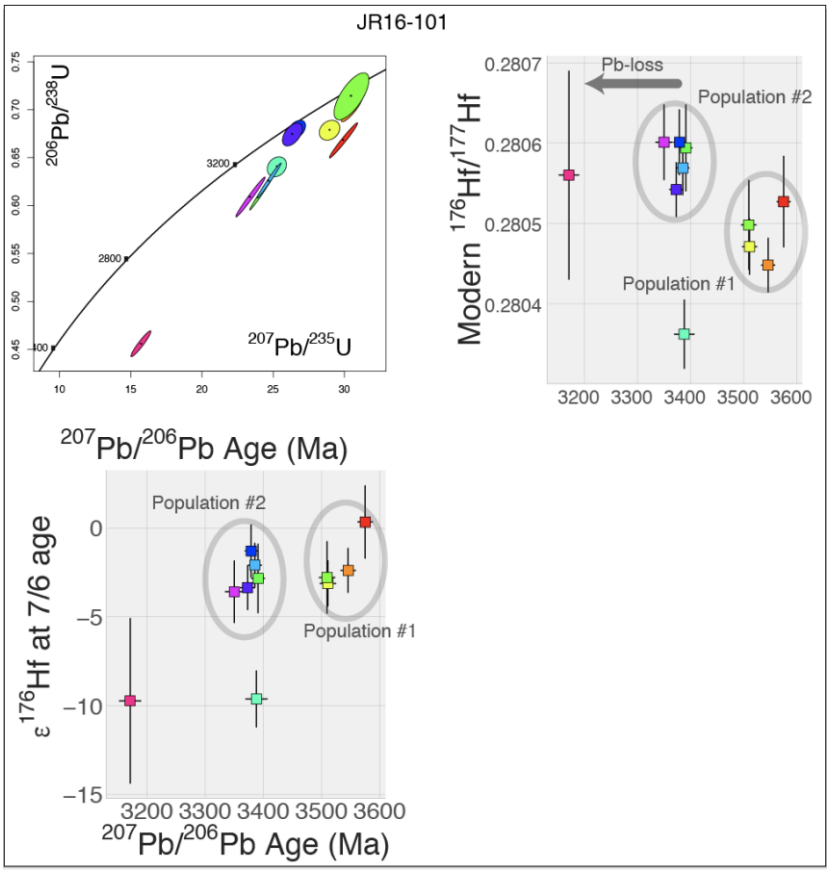

Figure S-4 Split-stream U-Pb-Hf data for sample JR16-101. This sample contains multiple populations of zircon growth, distinguishable by combining the U-Pb and Hf datasets. Symbol colours correspond to individual analyses. The oldest four analyses have distinctly unradiogenic Hf-isotope compositions, suggesting they are a distinct population from the main analyses. Therefore, we broke the analyses into two groups, with distinct ages and εHf values, shown in grey circles. The older population is interpreted to consist of inherited xenocrystic zircon cores, while the second population is interpreted to be the magmatic growth and true age of the rock.

Supplementary Tables

Tables S-1 and S-2 are available for download as Excel files from the online version of the article at http://www.geochemicalperspectivesletters.org/article1907.

Table S-1 Whole-rock major, minor, and trace-element compositions of the samples presented here. The table also includes GPS coordinates for each sample, as well as the average Age and εHf value, determined by zircon LA-ICPMS analysis.

Table S-2 Zircon U-Pb-Hf data. Table S-2a presents the U-Pb-Hf data for standard zircons analysed during each sequence, while Table S-2b presents the U-Pb-Hf isotopic data from the unknowns.

Supplementary Information References

Amelin, Y., Lee, D.C., Halliday, A.N., Pidgeon, R.T. (1999) Nature of the Earth's earliest crust from hafnium isotopes in single detrital zircons. *Nature* 399, 252–255.

Amelin, Y., Lee, D.C., Halliday, A.N. (2000) Early-middle Archaean crustal evolution deduced from Lu-Hf and U-Pb isotopic studies of single zircon grains. *Geochimica et Cosmochimica Acta* 64, 4205–4422.

Bauer, A.M., Fisher, C.M., Vervoort, J.D., Bowring, S.A. (2017) Coupled zircon Lu–Hf and U–Pb isotopic analyses of the oldest terrestrial crust, the >4.03 Ga Acasta Gneiss Complex. *Earth and Planetary Science Letters* 458, 37–48.

Bleeker, W., Ketchum, J.W., Jackson, V.A., Villeneuve, M.E. (1999) The Central Slave Basement Complex, Part I: its structural topology and autochthonous cover. *Canadian Journal of Earth Sciences* 36, 1083–1109, doi: 10.1139/e98-102.

Fisher, C.M., Vervoort, J.D., Hanchar, J.M, (2011) Synthetic zircon doped with hafnium and rare earth elements: A reference material for in situ hafnium isotope analysis. *Chemical Geology* 286, 32–47.

Guitreau, M., Blichert-Toft, J., Martin, H., Mojzsis, S.J. (2012) Hafnium isotope evidence from Archean granitic rocks for deep-mantle origin of continental crust. *Earth and Planetary Science Letters* 337-338, 211–223

Guitreau, M., Blichert-Toft, J., Mojzsis, S.J., Roth, A.S.G., Bourdon, B., Cates, N.L., Bleeker, W. (2014) Lu–Hf isotope systematics of the Hadean–Eoarchean Acasta Gneiss Complex (Northwest Territories, Canada). *Geochimica et Cosmochimica Acta* 135, 251–269.

Ickert, R.B. (2013) Algorithms for estimating uncertainties in initial radiogenic isotope ratios and model ages. *Chemical Geology* 340, 131–138.

Iizuka, T., Hirata, T. (2005) Improvements of precision and accuracy in in situ Hf isotope microanalysis of zircon using the laser ablation-MC-ICPMS technique. *Chemical Geology* 220, 121–137.

Iizuka, T., Komiya, T., Johnson, S.P., Kon, Y., Maruyama, S., Hirata, T. (2009) Reworking of Hadean crust in the Acasta gneisses, northwestern Canada: Evidence from in-situ Lu–Hf isotope analysis of zircon. *Chemical Geology* 259, 230–239.

Kemp, A.I.S., Wilde, S.A., Hawkesworth, C.J., Coath, C.D., Nemchin, A., Pidgeon, R.T., Vervoort, J.D., DuFrane, S.A. (2010) Hadean crustal evolution revisited: New constraints from Pb–Hf isotope systematics of the Jack Hills zircons. *Earth and Planetary Science Letters* 296, 45–56, doi: 10.1016/j.epsl.2010.04.043.

Pietranik, A.B., Hawkesworth, C.J., Storey, C.D., Kemp, A.I.S., Sircombe, K.N., Whitehouse, M.J., Bleeker, W. (2008) Episodic, mafic crust formation from 4.5 to 2.8 Ga: New evidence from detrital zircons, Slave craton, Canada. *Geology* 36, 875–878, doi: 10.1130/G24861A.1.

Reimink, J.R., Chacko, T., Stern, R.A., Heaman, L.M. (2016a) The birth of a cratonic nucleus: lithogeochemical evolution of the 4.02–2.94 Ga Acasta Gneiss Complex. *Precambrian Research* 281, 453–472, doi: 10.1016/j.precamres.2016.06.007.

Reimink, J.R., Davies, J.H.F.L., Chacko, T., Stern, R.A., Heaman, L.M., Sarkar, C., Schaltegger, U., Creaser, R.A., Pearson, D.G. (2016b) No evidence for Hadean continental crust within Earth's oldest evolved rock unit. *Nature Geoscience* 9, 777–780.

Thorpe, R.I., Cumming, G.L., and Mortensen, J.K., 1992, A Significant Pb Isotope Boundary in the Slave Province and Its Probable Relation To Ancient Basement in the western Slave Province. Geological Survey of Canada Open File report, 2484, 179-184.

Vervoort, J.D., Kemp, A.I.S. (2016) Clarifying the zircon Hf isotope record of crust–mantle evolution. *Chemical Geology* 425, 65–75.

Vermeesch, P. (2018) IsoplotR: a free and open toolbox for geochronology. *Geoscience Frontiers*, doi: 10.1016/j.gsf.2018.04.001.

Yamashita, K., Creaser, R.A., Stemler, J.U., Zimaro, T.W. (1999) Geochemical and Nd-Pb isotopic systematics of late Archean granitoids, southwestern Slave Province, Canada: constraints for granitoid origin and crustal isotopic structure. *Canadian Journal of Earth Sciences* 36, 1131–1147, doi: 10.1139/e98-047.